

# Three-Phase Mixed-Wet Capillary Pressure Curves From A Bundle-Of-Triangular-Tubes Model

Johan O. Helland\* and Svein M. Skjæveland

*Stavanger University College, P.O. Box 8002, N-4068 Stavanger, Norway*

---

## Abstract

We present a bundle-of-triangular-tubes model that simulates three-phase mixed-wet capillary pressure curves for any sequences of gas, oil, and water invasion processes. We use expressions for the capillary entry pressures that truly accounts for the mixed wettability condition and the possibility of simultaneous displacement of the fluids occupying the cross-sections. As a consequence, invasion does not necessarily proceed in the order of monotonic increasing or decreasing pore size. A diversity of cross-sectional fluid configurations may occur because of pore shape and different combinations of the contact angles. The applicability range of the model is demonstrated by simulations of different sequences of the invasion processes. For a given set of interfacial tensions we study the saturation dependencies on the capillary pressures. In general we find that all capillary pressures depend on two saturations, although the saturation dependency is affected by the process type, the saturation history, and the wettability. For water-wet and mixed-wet conditions the oil-water capillary pressure may only depend on the water saturation, whereas for oil-wet conditions the gas-oil capillary pressure may only depend on the oil saturation.

*Key words:* Three-phase, Mixed wettability, Bundle-of-triangular-tubes, Capillary pressure

---

## 1 Introduction

To describe three-phase transition zones and the dynamics of water-oil and gas-oil contact movements, a three-phase capillary pressure correlation is needed for mixed-wet reservoirs. The correlation should be based on sound physical principles yet sufficiently simple to be included in a reservoir simulator. In the reservoir, situations may occur where one of the phases appears or disappears, e.g., transitions

---

\* Corresponding author.

between gas and oil phase in condensate reservoirs, or when zero residual oil saturation is approached by drainage through connected layers. The correlation should be designed to account for a smooth transition between two- and three-phase flow to accommodate these situations.

Three-phase capillary pressure vs. saturation relationships have traditionally been predicted from corresponding two-phase measurements. However, both experimental and numerical work have shown that this approach is not always valid. Hence, there is a need for direct measurements of three-phase capillary pressure relationships to develop reliable correlations. There is a paucity of data reported in the literature. To our knowledge, measurements with three varying saturations have only been reported by Kalaydjian (1992). He measured three-phase drainage and imbibition capillary pressures in water-wet sandstone core samples. Bradford and Leij (1995a,b, 1996) measured three-phase capillary pressures in sandpacks for several wetting conditions achieved by mixing different fractions of water-wet and oil-wet sands. In these experiments, however, one saturation was kept fixed.

As there are few measured three-phase capillary data available, we have chosen the route of adding artificially generated data from a simple simulation model. Because of two independent saturations, there is an infinite number of possible three-phase displacement processes. The trajectory of a specific process in the saturation space is determined by the three capillary pressures. A simulation model that produces realistic capillary pressure curves may be used to predict processes not covered by time-consuming measurements. We choose to represent the pore network by a bundle-of-tubes model, the tubes having triangular, equilateral cross-sections. The model is programmed in MATLAB<sup>†</sup> and has been shown to produce realistic two-phase capillary pressure curves for mixed-wet rock, scanning loops included (Heland and Skjæveland, 2004).

The triangular pore shape allows for representation of physical processes such as the development of mixed wettability within a single pore (Kovscek et al., 1993; Hui and Blunt, 2000) and oil drainage through layers in the crevices (Hui and Blunt, 2000; Dong et al., 1995; Keller et al., 1997). The possibility of simultaneous occupancy of more than one fluid phase in the cross-sectional area of a triangular tube requires analysis of the fluid configurations and accurate calculation of the capillary entry pressures accounting for all possible displacements. Recently, van Dijke and Sorbie (2003) derived a general formula for three-phase capillary entry pressures into tubes with angular cross-sections accounting for simultaneous displacement of all phases. However, they did only consider pores of uniform wettability. We extend the method to account for mixed-wet tubes from the two-phase derivation given by Ma et al. (1996). Along with the derivations we propose an algorithm that determines which type of displacement that may occur for the different combinations of the contact angles.

---

<sup>†</sup> MATLAB is a registered trademark of TheMathWorks Inc.

In the present paper, we describe the three-phase bundle-of-triangular-tubes model. The flexibility of the model is demonstrated by several numerical experiments at different wetting conditions and different sequences of gas, oil, and water invasion processes. The simulations are presented as three-phase capillary pressure surfaces and iso-capillary pressure curves (“iso-caps”), from which the saturation dependencies are inferred.

## 2 Preliminaries

The wetting preference of a solid surface in contact with two fluids is typically characterized by the contact angle. Assuming that the denser phase  $j$  is wetting relative to phase  $i$ , then  $\cos \theta_{ij} \geq 0$ , where the contact angle  $\theta_{ij}$  is measured through phase  $j$ . The wetting order in a three-phase fluid system of oil, water and gas may be divided into three categories (Hui and Blunt, 2000; Zhou and Blunt, 1998):

- In water-wet media, water is wetting, oil intermediate-wetting, and gas non-wetting. The contact angles satisfy  $\theta_{ow} \leq \frac{\pi}{2}$ ,  $\theta_{go} \leq \frac{\pi}{2}$ , and  $\theta_{gw} \leq \frac{\pi}{2}$ .
- In weakly oil-wet media, oil is wetting, water intermediate-wetting, and gas non-wetting ( $\theta_{ow} > \frac{\pi}{2}$ ,  $\theta_{go} \leq \frac{\pi}{2}$ , and  $\theta_{gw} \leq \frac{\pi}{2}$ ).
- In strongly oil-wet media, oil is wetting, gas intermediate-wetting, and water non-wetting ( $\theta_{ow} > \frac{\pi}{2}$ ,  $\theta_{go} \leq \frac{\pi}{2}$ , and  $\theta_{gw} > \frac{\pi}{2}$ ).

Recently, van Dijke and Sorbie (2002) proposed linear relationships of  $\cos \theta_{go}$  and  $\cos \theta_{gw}$  as functions of  $\cos \theta_{ow}$  accounting for the above wetting orders:

$$\cos \theta_{go} = \frac{1}{2\sigma_{go}}(C_{so} \cos \theta_{ow} + C_{so} + 2\sigma_{go}), \quad (1)$$

and

$$\cos \theta_{gw} = \frac{1}{2\sigma_{gw}}((C_{so} + 2\sigma_{ow}) \cos \theta_{ow} + C_{so} + 2\sigma_{go}), \quad (2)$$

where the oil spreading coefficient  $C_{so} = \sigma_{gw} - \sigma_{go} - \sigma_{ow}$  is nonpositive and reflects the interfacial tensions measured at thermodynamic equilibrium. Thus assuming that the underlying wettability is known in terms of the oil-water contact angles, calculations of  $\theta_{go}$  and  $\theta_{gw}$  are possible by Eqs. (1), (2).

An important feature of the capillary behavior in an angular tube is the possibility of simultaneous occupancy of more than one fluid in the cross-section. The prevailing cross-sectional fluid configuration depends on the pore shape, the contact angles, and the capillary pressures. Expressions for the two-phase capillary entry pressures are derived by the MS-P method, named after the contributions from Mayer and Stowe (1965) and Princen (1969a,b, 1970). This method is founded on an energy balance equation which equates the virtual work with the associated change of surface free energy for a small displacement of the interface in the direction along

the tube. The energy balance equation then relates the entry radius of curvature to the cross-sectional area exposed to change of fluid occupancy, the bounding cross-sectional fluid-solid and fluid-fluid lengths, and the contact angle.

Following this approach, Ma et al. (1996) derived the capillary entry pressures for primary drainage and imbibition for mixed-wet, regular,  $n$ -sided tubes. The analysis for this geometry is largely simplified as all corners have the same half-angle  $\alpha$  and hence the same fluid configuration. There are two scenarios that need to be considered separately depending on the contact angle. As an example, consider invasion of phase  $i$  into a uniformly wetted tube initially filled with the denser phase  $j$ . If

$$\theta_{ij} < \frac{\pi}{2} - \alpha, \quad (3)$$

phase  $i$  occupies the bulk area while phase  $j$  is still residing in the corners. If the contact angle does not satisfy Eq. (3), phase  $i$  occupies the entire cross-section during invasion. The invading interface separating the bulk fluids is referred to as the main terminal meniscus (MTM), and the interface separating bulk fluid from corner fluid, if present, is referred to as the arc meniscus (AM). The curvature of an AM is represented by a cross-sectional circular arc of radius  $r_{ij}$ . Thus, by Young-Laplace's equation, the capillary pressure may be expressed as

$$P_{cij} = \frac{\sigma_{ij}}{r_{ij}}. \quad (4)$$

In a three-phase system the capillary pressures are, by definition, related to each other by

$$P_{cgw} = P_{cgo} + P_{cow}. \quad (5)$$

The application of Eq. (4) on all capillary pressures then yields the useful relation

$$\frac{\sigma_{gw}}{r_{gw}} = \frac{\sigma_{go}}{r_{go}} + \frac{\sigma_{ow}}{r_{ow}}. \quad (6)$$

Hence, if two of the radii of curvature are known, we may calculate the third from Eq. (6).

### 3 Model description

The pore network is represented as a bundle of parallel tubes, the tubes having equilateral, triangular cross-sections. The geometry of an equilateral triangle is readily described by the half-angle of the corner,  $\alpha = \frac{\pi}{6}$ , and the radius of the inscribed circle  $R$ . We assume that the pore-size frequency is described by a truncated two-parameter Weibull distribution. This is a flexible distribution that has been employed frequently for this purpose (Diaz et al., 1987; Fenwick and Blunt,

1998; Hui and Blunt, 2000). The pore sizes  $R$  are selected from the cumulative distribution function in the following manner: Pick random numbers  $x \in [0, 1]$  and calculate the inscribed radius from

$$R = R_{ch} \left( -\ln[(1-x) \exp(-\left[\frac{R_{max} - R_{min}}{R_{ch}}\right]^\eta) + x] \right)^{\frac{1}{\eta}} + R_{min}, \quad (7)$$

where  $R_{max}$ ,  $R_{min}$  and  $R_{ch}$  are the inscribed radii of the largest, smallest and characteristic pore sizes, respectively, and  $\eta$  is a dimensionless parameter.

The model is programmed to simulate gas, oil and water invasion processes in any sequence starting with primary drainage of a waterfilled and water-wet medium. An invasion process is simulated by increasing or decreasing a capillary pressure stepwise until some maximum or minimum value is reached. At each step the fluid occupancies in the tubes are updated and the saturation is calculated. Invasion of the oil phase is simulated by increasing  $P_{cow}$  at a constant  $P_{cgw}$ . At each pressure step  $P_{cgo}$  is calculated from Eq. (5). During water invasion  $P_{cow}$  is decreased at a constant  $P_{cgo}$ , and  $P_{cgw}$  is calculated by Eq. (5). During gas invasion  $P_{cgo}$  is increased, and  $P_{cgw}$  is calculated from Eq. (5) assuming a constant  $P_{cow}$ . To simulate a predetermined sequence of several gas, oil and water invasion processes, a list of capillary pressures is specified where each value corresponds to the capillary pressure at which the specific process is terminated.

Initially all tubes are waterfilled and strongly water-wet, and hence the contact angle during primary drainage,  $\theta_{pd}$ , is always small and satisfies Eq. (3). It is assumed that oil always contacts the pore walls of the invaded tubes, and hence the sides may experience a wettability alteration while the corners remain water-wet. The final configuration of a tube after primary drainage is shown in Fig. 1. The distance  $b_{pd}$  of the solid surface that remains water-wet is given by

$$b_{pd} = \frac{\sigma_{ow} \cos(\theta_{pd} + \alpha)}{P_{cow}^{max} \sin \alpha}, \quad (8)$$

where  $P_{cow}^{max}$  is the capillary pressure at the end of primary drainage.

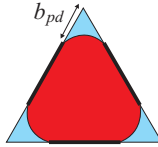


Figure 1. Final configuration of a tube after primary drainage. The bold lines along the sides represent the lengths of the pore wall where the wettability may have changed. The distances  $b_{pd}$  in the corners remain water-wet.

The amount of contact angle hysteresis between primary drainage, imbibition and secondary drainage is affected by the degree of wettability alteration and the surface roughness (Morrow, 1975; Yang et al., 1999). To accommodate this we allow all

receding and advancing oil-water contact angles,  $\theta_{owr}$  and  $\theta_{owa}$  respectively, that satisfy  $\theta_{pd} \leq \theta_{owr} \leq \theta_{owa}$ . If gas displaces oil and water, the gas-oil and gas-water interfaces are receding with contact angles  $\theta_{gor}$  and  $\theta_{gwr}$  calculated from Eqs. (1), (2) with  $\theta_{ow} = \theta_{owr}$ . Similarly, oil and water displaces gas with advancing contact angles  $\theta_{goa}$  and  $\theta_{gwa}$  calculated from Eqs. (1), (2) assuming  $\theta_{ow} = \theta_{owa}$ .

#### 4 Fluid configurations

The model allows for simulations of any sequence of the invasion processes starting with primary drainage. Contact angle hysteresis then leads to a diversity of possible fluid configurations that have to be analyzed individually. The number of configurations are restricted by several assumptions. We allow maximum two AMs to be present on the surface exposed to a potential wettability change. An additional AM may be located at position  $b_{pd}$ . We do not study situations where the gas pressure is large enough for gas invasion into tubes, and corners of tubes, where oil has never been. As a consequence, any gas-water AMs located at position  $b_{pd}$  are hinging with contact angles varying with  $P_{cgw}$ . Oil-water AMs located at this position are allowed to move on to the water-wet surface when the hinging contact angle has reached  $\theta_{pd}$ . This happens when  $P_{cow} = P_{cow}^{\max}$ , and a further increase of  $P_{cow}$  causes the length of the water-wet surface,  $b_{pd}$ , to decrease additionally. The AMs located on the surface of altered wettability may also hinge at fixed positions while the contact angles change with capillary pressure. If the advancing or receding contact angles are attained, the AMs begin to move with constant contact angles during a further decrease or increase of the capillary pressure, respectively. Oil is always assumed to be wetting relative to gas, i.e.,  $\theta_{go} < \frac{\pi}{2}$ , and hence only the three aforementioned wetting orders are considered. This implies that bulk oil can not be bounded by gas layers in the cross-sections. With these assumptions we find that the 17 configurations presented in Fig. 2 may occur during the simulations.

During the two-phase oil/water saturation history the configurations A–G may appear. Configuration A shows a tube that has always been waterfilled. Configuration B and C occur during waterflooding when the water content in the corners has started to increase after primary drainage. Water invasion into configuration B results in configuration D, while invasion into configuration C may result in either configuration D or E. Configuration F may appear during secondary drainage when oil invades configuration E and the contact angle hysteresis is large. If configuration B occurs for the first time during secondary drainage, a subsequent waterflooding may result in configuration G. Helland and Skjæveland (2004) provided a detailed description of the two-phase oil/water invasion processes, including expressions for the capillary entry pressures and the layer collapse capillary pressures. If the oil saturation has become zero, and only gas and water invasion processes are considered, the treatment of configuration H–L is analogous to the corresponding two-phase oil/water situation.

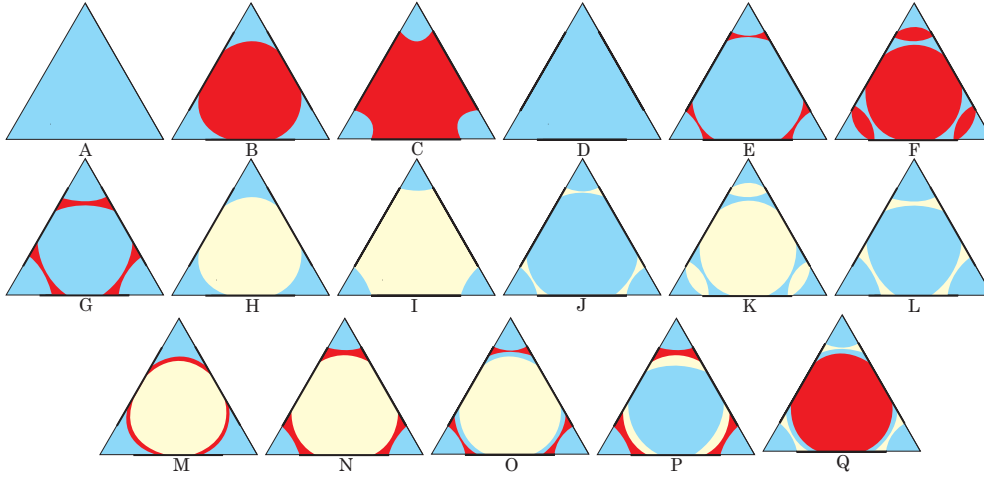


Figure 2. Fluid configurations for any sequences of the invasion processes, with water in blue, oil in red, and gas in yellow. The bold lines along the sides represent the lengths with potentially altered wettability. Oil is always assumed to be wetting relative to gas.

When a configuration containing two of the phases is invaded by the third phase, several displacements are possible. Which displacement to occur are determined by the combination of the capillary pressures and the contact angles. The algorithm used to determine the displacements and the associated expressions for the capillary entry pressures are described in the Appendix A for configuration E as the illustrating example. The treatment of the other configurations is similar. Gas invasion into configuration B, C, or E may be a displacement to configuration M, N, or O, respectively. A subsequent waterflooding of configuration N may result in configuration P, and oil invasion into configuration J may be a displacement to configuration Q. The number of possible displacements is reduced if the invading phase is already present as layers. As an example, water invasion into configuration O is always a displacement to configuration E, while oil invasion into configuration O is always a displacement to configuration C or F. The fluid layers are assumed to collapse when the bounding AMs meet at the contact lines or the midpoints. We employ the expressions derived by Hui and Blunt (2000) for the collapse of fluid layers in a three-phase configuration.

## 5 Numerical experiments

We have performed several simulations for different sequences of oil, water and gas invasion processes to demonstrate the flexibility of the model and to analyze the saturation dependencies of the capillary pressures. The simulations are conducted on a bundle of 2000 tubes. The pore sizes are calculated from Eq. (7) assuming  $R_{\min} = 1\mu\text{m}$ ,  $R_{\max} = 100\mu\text{m}$ ,  $R_{\text{ch}} = 20\mu\text{m}$  and  $\eta = 2$ . We consider a fluid system with the interfacial tensions  $\sigma_{go} = 0.015\text{ N/m}$ ,  $\sigma_{ow} = 0.025\text{ N/m}$  and  $\sigma_{gw} = 0.035\text{ N/m}$ , representing realistic values for a system of water, crude oil

and natural gas (Whitson and Brulè, 2000). Three different wettability conditions are modelled, and the contact angles for each case are presented in Table 1. We assume randomly distributed contact angles  $\theta_{owa}$  to accommodate realistic situations where the rock surfaces may be composed of mineralogical substances with different affinity to crude oil. For convenience, the receding contact angle  $\theta_{owr}$  is set to a certain fraction of  $\theta_{owa}$ . The advancing and receding gas-oil and gas-water contact angles are calculated from Eqs. (1), (2), respectively.

Although the model allows for any two-phase oil-water saturation history starting with primary drainage, we have decided to introduce the gas phase after the first imbibition in all simulations. The specific numerical experiments performed are as follows:

- Gas invasion at constant  $P_{cow}$  for the three cases of wettability.
- Water invasion at constant  $P_{cgo}$  after gas invasion (only mixed-wet case).
- Two examples of gas invasion when all the capillary pressures are allowed to vary (only mixed-wet case).

Wettability case	$\theta_{pd}$	$\theta_{owa}$	$\theta_{owr}$
Water-wet	$0^\circ$	$[45^\circ, 90^\circ]$	$0.7\theta_{owa}$
Mixed-wet	$0^\circ$	$[60^\circ, 180^\circ]$	$0.7\theta_{owa}$
Oil-wet	$0^\circ$	$[130^\circ, 180^\circ]$	$0.8\theta_{owa}$

Table 1

Contact angles for the three different wetting conditions.

Each experiment is run from several initial saturations. The three-phase capillary pressure – saturation data from the simulations constitute capillary pressure surfaces in a three-dimensional space spanned by two saturations and the capillary pressure. We present two-dimensional plots of iso-caps in the saturation space in addition to saturation paths for the simulations.

Fig. 3 shows the saturation trajectories and the gas-oil and gas-water iso-caps for gas invasion with constant  $P_{cow}$  for the three cases of variable wettability. In these experiments the saturation paths are identical to the oil-water iso-caps since  $P_{cow}$  is constant along each trajectory. By Fig. 3(a)–(c), it is shown that  $P_{cow}$  displays a stronger dependency on the oil saturation as the conditions become more oil-wet. For the water-wet and mixed-wet cases  $P_{cow}$  depends only on the water saturation except for small oil saturations. The gas-oil capillary pressure also shows a stronger dependency on the oil saturation as the conditions become more oil-wet, see Fig. 3(d)–(f). For water-wet and mixed-wet conditions  $P_{cgo}$  is clearly a function of two saturations, whereas for the oil-wet case  $P_{cgo}$  is a function of only the oil saturation except for small gas saturations. The gas-water capillary pressure depends on two saturations in all cases, as shown in Fig. 3(g)–(i), although a slightly stronger dependency on the gas saturation is seen for the oil-wet case.

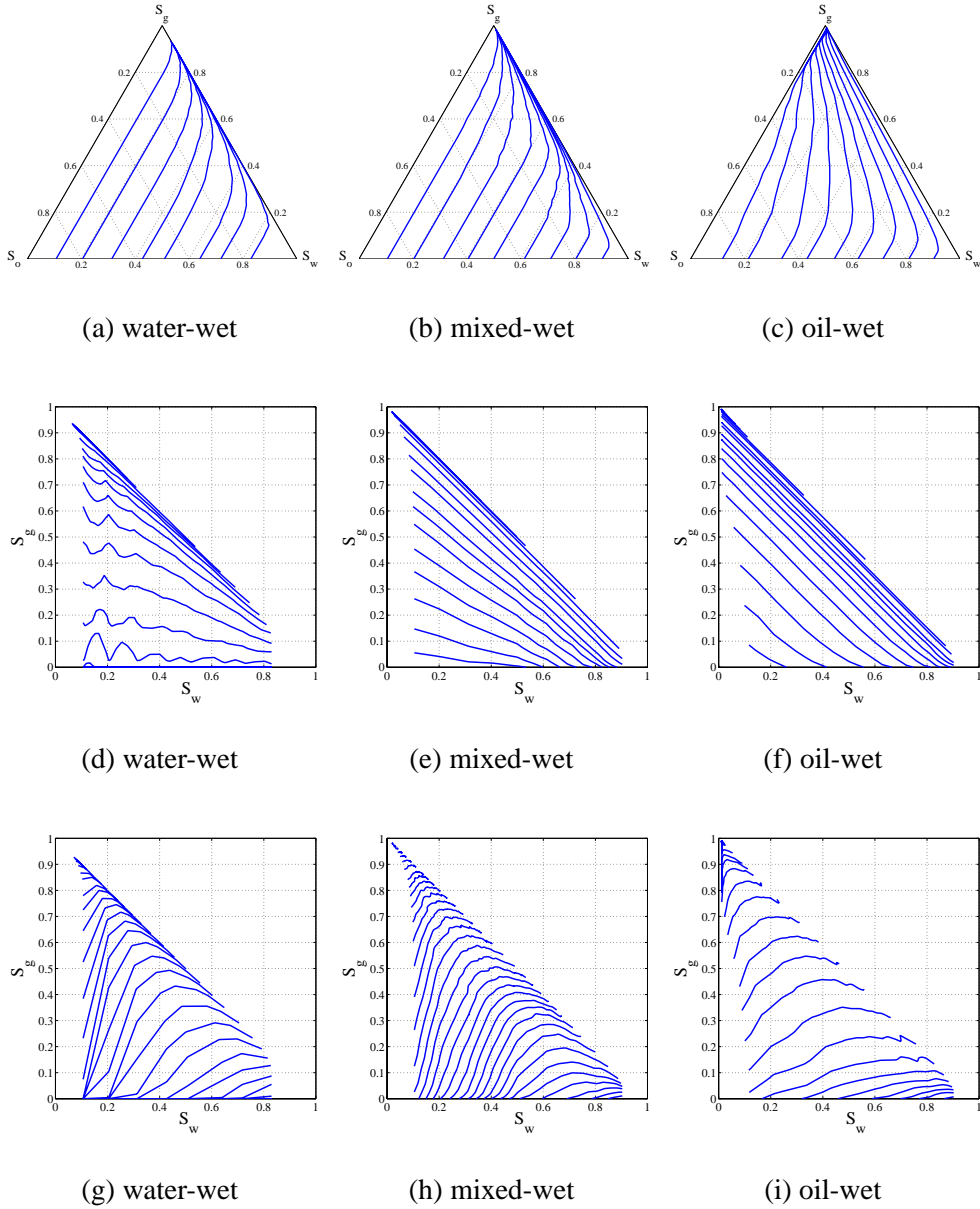


Figure 3. Gas invasion with constant  $P_{cow}$ : (a)–(c) saturation trajectories. (d)–(f) gas-oil iso-caps. (g)–(i) gas-water iso-caps.

The strong dependency on the water saturation that  $P_{cow}$  exhibits for the water-wet case as compared with the strong dependency on the oil saturation by  $P_{cgo}$  for the oil-wet case is explained by the change of wetting order of the three phases. The capillary pressure between the wetting and intermediate-wetting phases appears to be a function of only the saturation of the wetting phase for strongly wetting conditions.

Water injection following gas injection (WAG) is a sequence of processes to increase oil recovery in the reservoirs. The saturation trajectories and the gas-water

and oil-water iso-caps for the water invasion simulations, mixed-wet case, are presented in Fig. 4. The water invasion is initiated from saturations along a gas invasion trajectory presented in Fig. 3(b). The gas-oil capillary pressure is constant during the water invasion, and hence the saturation trajectories are identical to the gas-oil iso-caps. In this case all three capillary pressures are functions of two saturations, although a strong water saturation dependency of  $P_{cow}$  and  $P_{cgw}$  is observed.

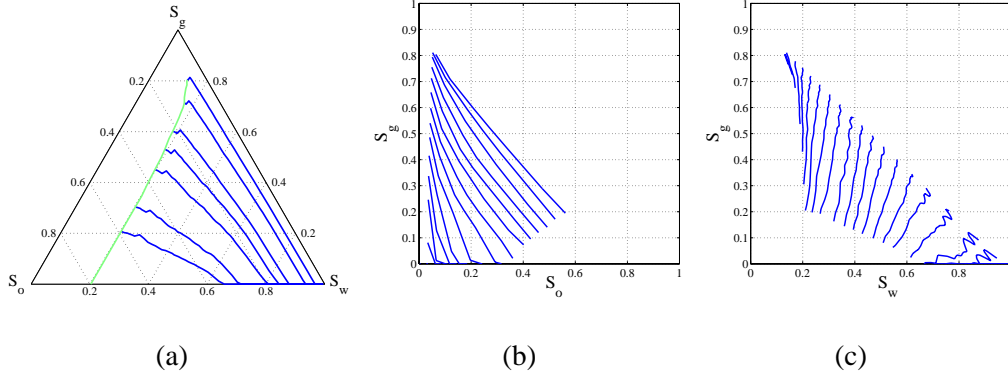
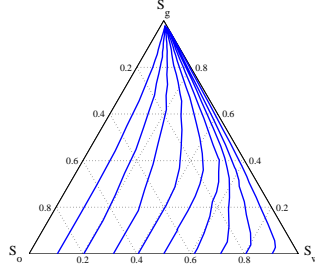


Figure 4. Water invasion with constant  $P_{cgo}$  starting from a gas invasion trajectory (mixed-wet case). (a) saturation paths. (b) oil-water iso-caps. (c) gas-water iso-caps.

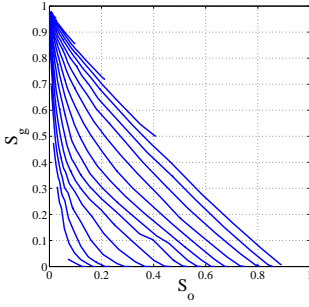
So far we have considered processes where one of the capillary pressures is held constant. As this may not be a realistic situation in the reservoir or in capillary pressure measurements conducted on core samples, we include simulations for the mixed-wet case where all capillary pressures are allowed to vary. For convenience, we have chosen a linear relationship between the capillary pressures. This is a scenario relevant for measurements performed by the centrifuge method where all the capillary pressures are proportional to each other (Virnovsky and Iversen, 1999). However, rather than imitate centrifuge experiments, we have decided to consider the effect of a variable  $P_{cow}$  during gas invasion. In the case of an increasing  $P_{cow}$  we assume that  $P_{cgo}$  is related to  $P_{cow}$  by

$$P_{cgo} = P_{cgo}^{\text{init}} + 2P_{cow}, \quad (9)$$

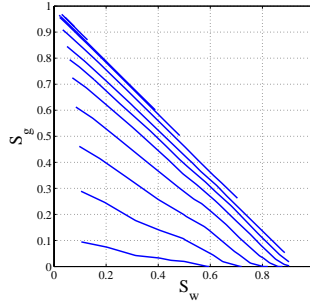
where  $P_{cgo}^{\text{init}}$  is the lowest gas-oil capillary entry pressure. The linear relationship is approximated as follows: Specify small and uniform increments of  $P_{cow}$  and calculate the corresponding increments of  $P_{cgo}$  from Eq. (9). A sequence of alternate increments of  $P_{cgo}$  and  $P_{cow}$  is assumed resulting in alternate gas and oil invasion processes. A specific invasion process is terminated when the associated capillary pressure increment is reached. Fig. 5 shows the saturation trajectories, the iso-caps and the capillary pressure surfaces generated from simulations satisfying Eq. (9). Not surprisingly, the saturation trajectories exhibit a more pronounced decrease of water saturation during the processes compared with the case of a constant  $P_{cow}$ . From Fig. 5(b) it is observed that  $P_{cow}$  depends on two saturations although the dependency on the water saturation still is strong. The other two capillary pressures



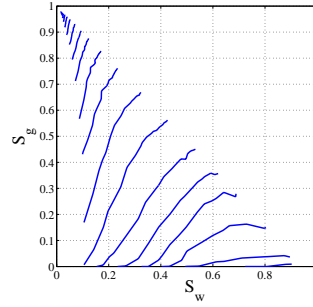
(a) saturation paths



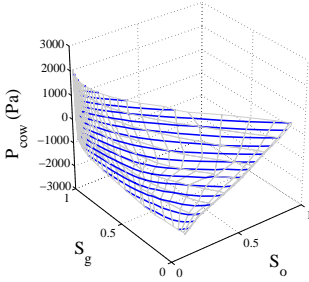
(b) oil-water iso-caps



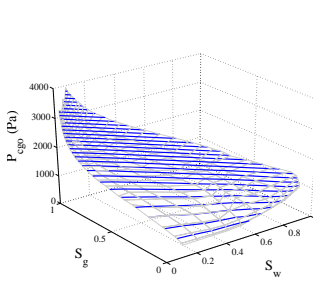
(c) gas-oil iso-caps



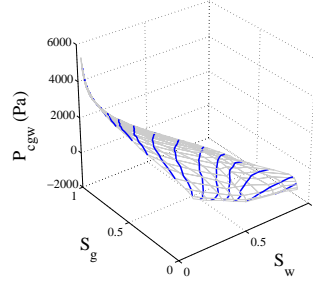
(d) gas-water iso-caps



(e)  $P_{cow}$



(f)  $P_{cgo}$



(g)  $P_{cgw}$

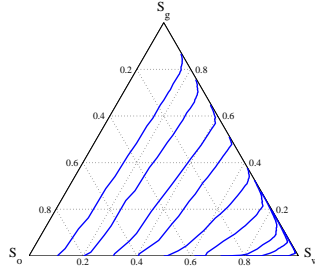
Figure 5. Saturation paths, iso-caps and capillary pressure surfaces for gas invasion simulations satisfying Eq. (9) (mixed-wet case).

are functions of two saturations.

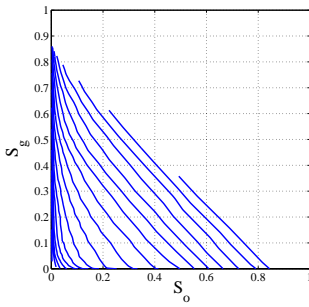
Finally, we consider a case with decreasing  $P_{cow}$  during gas invasion. We assume that for each trajectory  $P_{cgo}$  is related to  $P_{cow}$  by

$$P_{cgo} = P_{cgo}^{\text{init}} - \frac{3}{2}P_{cow}. \quad (10)$$

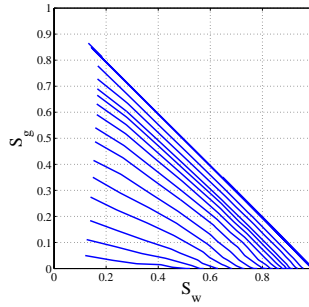
The simulation procedure is analogous to the previous example, except for alternate gas and water invasion processes. This is a scenario that may be close to a continuous WAG-injection process where both the gas and water saturations increase. The



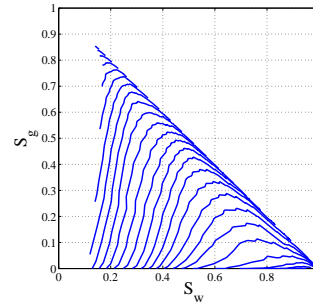
(a) saturation paths



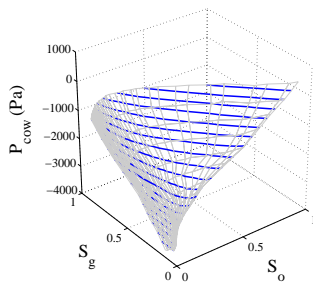
(b) oil-water iso-caps



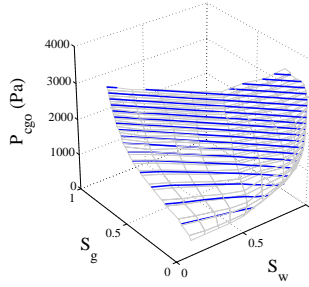
(c) gas-oil iso-caps



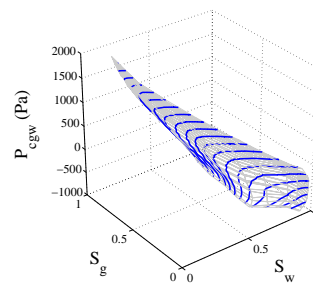
(d) gas-water iso-caps



(e)  $P_{cow}$



(f)  $P_{ego}$



(g)  $P_{cgw}$

Figure 6. Saturation paths, iso-caps and capillary pressure surfaces for gas invasion simulations satisfying Eq. (10) (mixed-wet case).

results are shown in Fig. 6. Again we find that the capillary pressures are functions of two saturations. Local variations in the shape of the iso-caps in Fig. 5(b)–(d) and Fig. 6(b)–(d) show that the saturation dependencies are affected by the functional relationship between the capillary pressures.

## 6 Discussion and further work

Three-phase flow processes at the pore scale depend in general on the saturation history and the capillary pressures. There is an infinite number of possible functional relationships between the three capillary pressures corresponding to an infinite number of unique saturation trajectories. Hence, it is an extremely ambitious task to develop three-phase capillary pressure correlations accounting for all possible processes. This points out the importance of a process-based approach as a foundation for the correlation development. This approach implies that the process is known in terms of the saturation trajectory or by the relationship between the three capillary pressures.

Work is in progress to measure three-phase capillary pressures by the porous plate and centrifuge methods (Virnovsky, 2004). The measurements may discern the regime of process types that may be appropriate for the correlation development. We plan to adjust the triangular tube model to reproduce the saturation paths from the measurements and check if the measured and simulated capillary pressure data agree. If a good match is obtained, we may conclude that the simulation model could be employed to predict capillary pressure curves within the same process regime as the measurements. The model could also be used to predict capillary pressure curves for a wider range of process types by extrapolating the measured data.

The time-consuming measurements and the numerous generic process types that may occur in the reservoir emphasize the utility value of a reliable simulation model that produces realistic three-phase capillary pressure curves for a wide range of processes. The functional form of the extensively validated Brooks-Corey correlation (Brooks and Corey, 1964; Skjæveland et al., 2000) has been shown to match the two-phase capillary pressure curves produced by the triangular tube model (Heland and Skjæveland, 2004). For primary drainage this correlation is written as

$$P_{cow} = cS_w^{-a}, \quad (11)$$

where  $c$  is the entry pressure and  $1/a$  the pore-size distribution index. The good match between the two-phase data and Eq. (11) may indicate that different combinations of several Brooks-Corey terms suffice to describe three-phase capillary pressure curves for different types of processes produced by the model. The shape of the curves obtained from intersections along saturation trajectories of the capillary pressure surfaces presented in Fig. 5(e)–(g) and Fig. 6(e)–(g) suggests that this approach may be promising.

## 7 Conclusions

- (1) A bundle-of-triangular-tubes model has been developed for simulation of three-phase capillary pressure curves for mixed-wet conditions for any sequences of gas, oil, and water invasion processes. Expressions are employed for the three-phase capillary entry pressures that truly account for the wettability conditions and the possibility of simultaneous displacement of the fluids occupying the cross-sections.
- (2) The saturation dependencies of the capillary pressures are in general affected by the saturation history, the process type and the wettability. In most cases we find that the capillary pressures depend on two saturations. For water-wet and mixed-wet conditions  $P_{cow}$  may only depend on the water saturation, whereas for oil-wet conditions  $P_{cgo}$  may only depend on the oil saturation.
- (3) The applicability range of the model is demonstrated by simulations of gas invasion while all the capillary pressures are allowed to vary.

## Nomenclature

- $a$  = Correlation parameter, see Eq. (11).
- $A$  = Cross-sectional tube area
- $b$  = Position of arc meniscus
- $c$  = Correlation parameter, see Eq. (11).
- $C_s$  = Spreading coefficient
- $C_1, C_2, C_3$  = Coefficients in polynomial, see Eqs. (A.21)–(A.23)
- $L_s$  = Cross-sectional fluid-solid length
- $L_f$  = Cross-sectional fluid-fluid length
- $P$  = Pressure
- $r$  = Radius of curvature
- $R$  = Radius of the inscribed circle
- $S$  = Saturation
- $W$  = Virtual work
- $x$  = Random number between 0 and 1
- $\alpha$  = Corner half angle
- $\beta$  = Angle defined from geometry of the AMs in the corners
- $\Delta F$  = Change of surface free energy
- $\delta x$  = Virtual displacement
- $\eta$  = Parameter in the Weibull distribution
- $\theta$  = Contact angle
- $\sigma$  = Interfacial tension

## Subscripts

- $a$  = Advancing

$c$  = Capillary  
 $ch$  = Characteristic  
 $g$  = Gas  
 $h$  = Hinging  
 $max$  = Maximum  
 $min$  = Minimum  
 $o$  = Oil  
 $pd$  = Primary drainage  
 $r$  = Receding  
 $w$  = Water

### *Superscripts*

$col$  = Collapse  
 $init$  = Initial  
 $max$  = Maximum  
(1) = Outermost AM in configuration E  
(2) = Innermost AM in configuration E

### *Abbreviations*

AM = Arc meniscus  
MS-P = Mayer and Stowe – Princen  
MTM = Main terminal meniscus  
WAG = Water alternate gas

## **Acknowledgements**

Support for Johan Olav Helland was provided by Statoil through the VISTA program.

## **A Appendix: Three-phase capillary entry pressures**

An algorithm is formulated to determine which displacement to occur during piston-like invasion for all combinations of the contact angles. For each type of displacement the corresponding capillary entry pressures are derived. The expressions are based on the derivation reported by van Dijke and Sorbie (2003). We extend the method to account for mixed wettability and contact angle hysteresis and hence the possibility of hinging AMs stuck at positions along the pore walls. For two-phase

flow, Helland and Skjæveland (2004) showed that invasion does not necessarily proceed in the order of monotonic increasing or decreasing pore size when the AMs are hinging. The capillary entry pressures are derived from an energy balance equation which equates the virtual work  $W$  with the corresponding change of surface free energy  $\Delta F$  for a small displacement of the MTM in the direction along the tube. The energy balance equation then relates the entry radius of curvature to the cross-sectional fluid occupancy, accounting for the possibility of simultaneous displacement of the fluids occupying the cross-section. We consider gas invasion into configuration E as an illustrating example. A paper is under preparation to provide a more complete analysis of the capillary entry pressures for other conditions.

The parameters of configuration E required for the derivation of the capillary entry pressures are as follows, see Fig. A.1(a):

$$\beta_{ow}^{(1)} = \frac{\pi}{2} - \alpha - \theta_{owh}^{(1)}, \quad (\text{A.1})$$

$$A_{ow}^{(1)} = \frac{R^2}{2 \tan \alpha} - \frac{r_{ow} b_{pd} \sin(\alpha + \beta_{ow}^{(1)})}{2} + \frac{r_{ow}^2 \beta_{ow}^{(1)}}{2}, \quad (\text{A.2})$$

$$L_{fow}^{(1)} = r_{ow} \beta_{ow}^{(1)}, \quad (\text{A.3})$$

$$L_{sow}^{(1)} = \frac{R}{\tan \alpha} - b_{pd}, \quad (\text{A.4})$$

$$\beta_{ow}^{(2)} = \frac{\pi}{2} + \alpha - \theta_{owh}^{(2)}, \quad (\text{A.5})$$

$$A_{ow}^{(2)} = \frac{R^2}{2 \tan \alpha} - \frac{r_{ow} b_{ow} \sin(\beta_{ow}^{(2)} - \alpha)}{2} - \frac{r_{ow}^2 \beta_{ow}^{(2)}}{2}, \quad (\text{A.6})$$

$$L_{fow}^{(2)} = r_{ow} \beta_{ow}^{(2)}, \quad (\text{A.7})$$

$$L_{sow}^{(2)} = \frac{R}{\tan \alpha} - b_{ow}, \quad (\text{A.8})$$

and

$$b_{ow} = \frac{r_{ow} \cos(\theta_{owh}^{(2)} - \alpha)}{\sin \alpha}, \quad (\text{A.9})$$

where the contact angle of the innermost AM is denoted  $\theta_{owh}^{(2)}$  to account for the possibility of a hinging AM before gas invasion.

Gas invasion into configuration E is a displacement to configuration I, N or O. In configuration N and O fluid layers form during invasion. A layer is assumed to collapse when the bounding AMs meet. The capillary pressure at which the water layer in configuration O collapses is given by

$$P_{cgw}^{\text{col}} = \begin{cases} P_{cow} \frac{\sigma_{gw} \cos \theta_{gwr} - \sin \alpha}{\sigma_{ow} \cos \theta_{owh}^{(2)} + \sin \alpha} & \text{if } \theta_{gwr} < \pi - \theta_{owh}^{(2)}, \\ P_{cow} \frac{\sigma_{gw} \cos(\theta_{gwr} + \alpha)}{\sigma_{ow} \cos(\theta_{owh}^{(2)} - \alpha)} & \text{if } \theta_{gwr} \geq \pi - \theta_{owh}^{(2)}. \end{cases} \quad (\text{A.10})$$

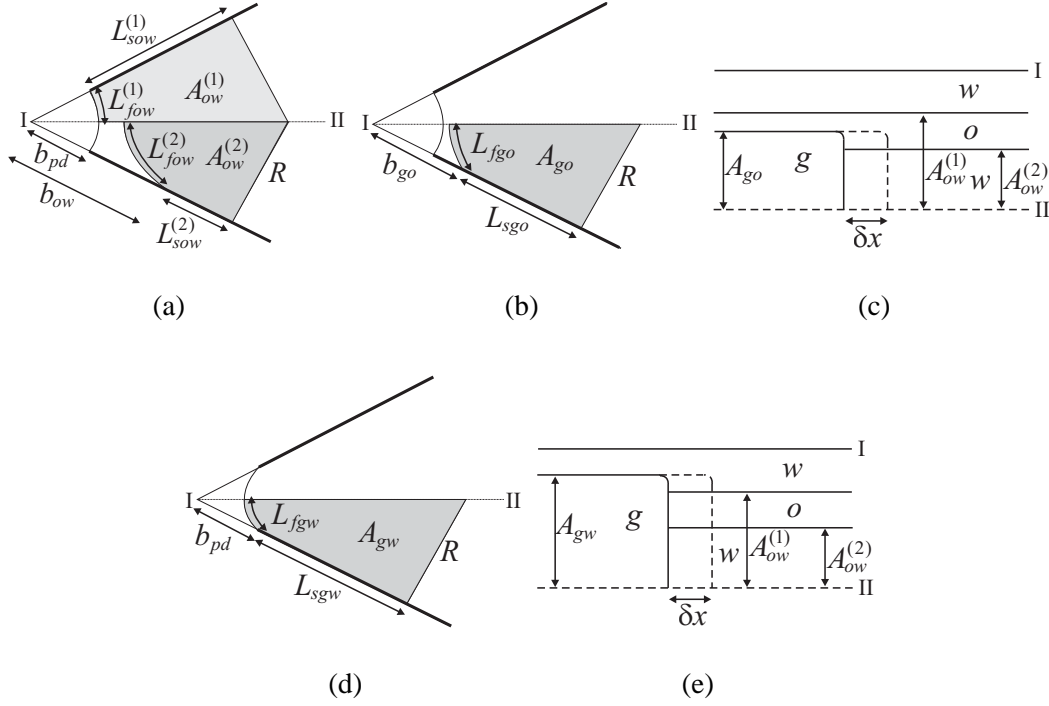


Figure A.1. Representation of the cross-sectional parameters of the fluid-fluid and fluid-solid interfaces. (a) configuration E. (b) configuration N. (c) displacement from configuration E to N. (d) configuration I. (e) displacement from configuration E to I.

The capillary pressure at which the oil layer in configuration N collapses is

$$P_{cgo}^{col} = \begin{cases} P_{cow} \frac{\sigma_{go} \cos \theta_{gor} - \sin \alpha}{\sigma_{ow} \cos \theta_{owh} - \sin \alpha} & \text{if } \theta_{gor} < \theta_{owh}^{(1)}, \\ P_{cow} \frac{\sigma_{go} \cos(\theta_{gor} + \alpha)}{\sigma_{ow} \cos(\theta_{owh}^{(1)} + \alpha)} & \text{if } \theta_{gor} \geq \theta_{owh}^{(1)}. \end{cases} \quad (\text{A.11})$$

We first consider the displacements and the associated capillary entry pressures when  $\theta_{gwr} < \frac{\pi}{2} - \alpha$ . In this case a displacement to configuration O is possible at a gas-water capillary entry pressure given by (Hui and Blunt, 2000)

$$P_{cgw} = \frac{\sigma_{gw}}{R} \left[ \cos \theta_{gwr} + \sqrt{\frac{\tan \alpha}{2} (\sin 2\theta_{gwr} - 2\theta_{gwr} - 2\alpha + \pi)} \right]. \quad (\text{A.12})$$

If  $P_{cgw} < P_{cgw}^{col}$ , the displacement is indeed from configuration E to O. If  $P_{cgw} \geq P_{cgw}^{col}$ , water layers do not form, and gas invasion may cause a simultaneous displacement of the fluids occupying the cross-section. In this case gas-oil-solid contact lines form, and the gas-oil contact angle affects the type of displacement occurring.

If  $\theta_{gor} < \frac{\pi}{2} - \alpha$ , formation of gas-oil AMs is possible, and hence a displacement

from configuration E to N is assumed. The corresponding energy balance equation,  $W = \Delta F$ , may be written as

$$\begin{aligned} \frac{\sigma_{gw}}{r_{gw}} A_{ow}^{(2)} + \frac{\sigma_{go}}{r_{go}} (A_{go} - A_{ow}^{(2)}) &= L_{sow}^{(2)} \sigma_{gw} \cos \theta_{gw} \\ &+ (L_{sgo} - L_{sow}^{(2)}) \sigma_{go} \cos \theta_{gor} + L_{fgo} \sigma_{go} - L_{fow}^{(2)} \sigma_{ow}, \end{aligned} \quad (\text{A.13})$$

where the capillary pressures are expressed in terms of the radii of curvature by Eq. (4). The cross-sectional occupancy after invasion is shown in Fig. A.1(b), and a view of the displacement in the direction along the tube is shown in Fig. A.1(c). The gas-oil parameters are as follows:

$$r_{go} = \frac{\sigma_{go}}{\frac{\sigma_{gw}}{r_{gw}} - \frac{\sigma_{ow}}{r_{ow}}}, \quad (\text{A.14})$$

$$A_{go} = \frac{R^2}{2 \tan \alpha} - \frac{r_{go} b_{go} \sin(\alpha + \beta_{go})}{2} + \frac{r_{go}^2 \beta_{go}}{2}, \quad (\text{A.15})$$

$$L_{sgo} = \frac{R}{\tan \alpha} - b_{go}, \quad (\text{A.16})$$

$$L_{fgo} = r_{go} \beta_{go}, \quad (\text{A.17})$$

$$r_{go} \sin \beta_{go} = b_{go} \sin \alpha, \quad (\text{A.18})$$

with  $\beta_{go}$  defined as

$$\beta_{go} = \frac{\pi}{2} - \alpha - \theta_{gor}. \quad (\text{A.19})$$

Inserting Eqs. (A.14)–(A.19) into Eq. (A.13) then yields a polynomial

$$C_1 r_{go}^2 + C_2 r_{go} + C_3 = 0, \quad (\text{A.20})$$

with the coefficients

$$C_1 = \frac{\sigma_{go}}{2} \left( \frac{\sin \beta_{go} \cos \theta_{gor}}{\sin \alpha} - \beta_{go} \right), \quad (\text{A.21})$$

$$C_2 = \frac{\sigma_{ow} A_{ow}^{(2)}}{r_{ow}} - L_{sow}^{(2)} \sigma_{gw} \cos \theta_{gwr} - \left( \frac{R}{\tan \alpha} - L_{sow}^{(2)} \right) \sigma_{go} \cos \theta_{gor} + L_{fow}^{(2)} \sigma_{ow}, \quad (\text{A.22})$$

and

$$C_3 = \sigma_{go} \frac{R^2}{2 \tan \alpha}. \quad (\text{A.23})$$

The correct solution for  $r_{go}$  has to agree with a position  $b_{go}$  of the invading gas-oil AM located between the apex of the corner and the position  $b_{ow}$  of the innermost oil-water AM. This condition may be formulated as

$$0 < r_{go} \leq \frac{b_{ow} \sin \alpha}{\sin \beta_{go}}. \quad (\text{A.24})$$

The solution  $r_{go}$  that satisfies Eq. (A.24) is used to calculate  $P_{cgo}$  by Eq. (4). If  $P_{cgo} < P_{cgo}^{\text{col}}$ , oil layers form, and the displacement is indeed from configuration E

to N. If  $P_{cgo} \geq P_{cgo}^{col}$ , the capillary entry pressure is calculated again assuming a displacement from configuration E to I. In this case the energy balance equation,  $W = \Delta F$ , is expressed as

$$\begin{aligned} \frac{\sigma_{gw}}{r_{gw}}(A_{gw} - A_{ow}^{(1)} + A_{ow}^{(2)}) + \frac{\sigma_{go}}{r_{go}}(A_{ow}^{(1)} - A_{ow}^{(2)}) = \\ L_{sow}^{(2)}\sigma_{gw} \cos \theta_{gwr} + (L_{sgw} - L_{sow}^{(2)})\sigma_{go} \cos \theta_{gor} \\ + L_{fgw}\sigma_{gw} - (L_{fow}^{(1)} + L_{fow}^{(2)})\sigma_{ow}, \end{aligned} \quad (\text{A.25})$$

where

$$A_{gw} = \frac{R^2}{2 \tan \alpha} - \frac{r_{gw} b_{pd} \sin(\alpha + \beta_{gw})}{2} + \frac{r_{gw}^2 \beta_{gw}}{2}, \quad (\text{A.26})$$

$$L_{sgw} = \frac{R}{\tan \alpha} - b_{pd}, \quad (\text{A.27})$$

$$L_{fgw} = r_{gw} \beta_{gw}, \quad (\text{A.28})$$

$$r_{gw} \sin \beta_{gw} = b_{pd} \sin \alpha, \quad (\text{A.29})$$

with  $\beta_{gw}$  defined as

$$\beta_{gw} = \frac{\pi}{2} - \alpha - \theta_{gwh}. \quad (\text{A.30})$$

The cross-sectional fluid occupancy after gas invasion is shown in Fig. A.1(d), and the displacement in the direction along the tube is shown in Fig. A.1(e). In this case the gas-water AMs are invading at position  $b_{pd}$  with an unknown hinging contact angle  $\theta_{gwh}$ . The capillary entry pressures are solved iteratively in the following manner: Assume  $r_{gw} = R$  as the initial value and calculate  $r_{go}$ ,  $A_{gw}$ ,  $L_{sgw}$ ,  $L_{fgw}$  and  $\beta_{gw}$  from Eqs. (A.14), (A.26)–(A.29). A new value of  $r_{gw}$  is obtained from Eq. (A.25). Finally,  $P_{cgo}$  and  $P_{cgw}$  are calculated from the converged values of  $r_{go}$  and  $r_{gw}$ .

When a displacement from configuration E to N is assumed, it is possible that none of the solutions of Eq. (A.20) satisfy Eq. (A.24). This is caused by a too high pressure in the layer phase (van Dijke and Sorbie, 2003). If this situation appears, the displacement to configuration N occurs while the gas-oil AMs are invading at position  $b_{go} = b_{ow}$  with a hinging contact angle  $\theta_{goh}$ . In this case  $L_{sgo} = L_{sow}^{(2)}$ , and hence the second term on the right-hand side of Eq. (A.13) vanishes. The entry radii of curvature are calculated iteratively from Eqs. (A.13)–(A.18), with  $\beta_{go}$  now defined as

$$\beta_{go} = \frac{\pi}{2} - \alpha - \theta_{goh}. \quad (\text{A.31})$$

Finally,  $P_{cgo}$  and  $P_{cgw}$  are obtained from the converged values of  $r_{go}$  and  $r_{gw}$ .

If  $\theta_{gor} \geq \frac{\pi}{2} - \alpha$ , the displacement to configuration I is assumed, and the capillary entry pressures are calculated by Eqs. (A.14), (A.25)–(A.29).

We have considered all displacements from configuration E when  $\theta_{gwr} < \frac{\pi}{2} - \alpha$ . If  $\theta_{gwr} \geq \frac{\pi}{2} - \alpha$ , formation of water layers is not possible, and hence the displacement

to configuration O does not occur. In this case gas-oil-solid contact lines form, and the analysis is identical to the above derivations for the different values of  $\theta_{gor}$ .

## References

- Bradford, S. A., Leij, F. J., 1995a. Fractional wettability effects on two- and three-fluid capillary pressure-saturation relations. *J. Cont. Hydr.* 20, 89–109.
- Bradford, S. A., Leij, F. J., 1995b. Wettability effects on scaling two- and three-fluid capillary pressure-saturation relations. *Env. Sci. Techn.* 29, 1446–1455.
- Bradford, S. A., Leij, F. J., 1996. Predicting two-and three-fluid capillary pressure-saturation relationships of porous media with fractional wettability. *Water Resources Research* 32 (2), 251–259.
- Brooks, R., Corey, A., 1964. Hydraulic properties of porous media. Hydraulic paper no. 3, Colorado State University .
- Diaz, C. E., Chatzis, I., Dullien, F. A. L., 1987. Simulation of capillary pressure curves using bond correlated site percolation on a simple cubic network. *Transport in Porous Media* 2, 215–240.
- Dong, M., Dullien, F. A. L., Chatzis, I., 1995. Imbibition of oil in film form over water present in edges of capillaries with an angular cross section. *J. Coll. Int. Sci.* 172, 21–36.
- Fenwick, D. H., Blunt, M. J., 1998. Three-dimensional modeling of three phase imbibition and drainage. *Adv. Water Resources* 25 (2), 121–143.
- Helland, J. O., Skjæveland, S. M., 2004. Physically-based capillary pressure correlation for mixed-wet reservoirs from a bundle-of-tubes model. Paper SPE 89428 presented at the SPE/DOE Fourteenth Symposium on Improved Oil Recovery, Tulsa, OK, Apr. 17–21 .
- Hui, M., Blunt, M. J., 2000. Effects of wettability on three-phase flow in porous media. *J. Phys. Chem. B* 104, 3833–3845.
- Kalaydjian, F. J.-M., 1992. Performance and analysis of three-phase capillary pressure curves for drainage and imbibition in porous media. Paper SPE 24878 presented at the SPE Annual Technical Conference and Exhibition, Washington, DC, Oct. 4–7 .
- Keller, A. A., Blunt, M. J., Roberts, P. V., 1997. Micromodel observation of the role of oil layers in three-phase flow. *Transport in Porous Media* 26, 277–297.
- Kovscek, A. R., Wong, H., Radke, C. J., 1993. A pore-level scenario for the development of mixed wettability in oil reservoirs. *Am. Inst. Chem. Eng. J.* 39 (6), 1072–1085.
- Ma, S., Mason, G., Morrow, N. R., 1996. Effect of contact angle on drainage and imbibition in regular polygonal tubes. *Coll. and Surf. A: Phys. and Eng. Asp.* 117, 273–291.
- Mayer, R. P., Stowe, R. A., 1965. Mercury porosimetry – breakthrough pressure for penetration between packed spheres. *J. Coll. Sci.* 20, 893–911.
- Morrow, N., 1975. The effects of surface roughness on contact angle with special

- reference to petroleum recovery. *J. Can. Pet. Tech.* 14 (4), 42–53.
- Princen, H. M., 1969a. Capillary phenomena in assemblies of parallel cylinders. i. capillary rise between two cylinders. *J. Coll. Int. Sci.* 30 (1), 69–75.
- Princen, H. M., 1969b. Capillary phenomena in assemblies of parallel cylinders. ii. capillary rise in systems with more than two cylinders. *J. Coll. Int. Sci.* 30 (3), 359–371.
- Princen, H. M., 1970. Capillary phenomena in assemblies of parallel cylinders. iii. liquid columns between horizontal parallel cylinders. *J. Coll. Int. Sci.* 34 (2), 171–184.
- Skjæveland, S., Siqveland, L., Kjosavik, A., Hammervold Thomas, W., Virnovsky, G., 2000. Capillary pressure correlation for mixed-wet reservoirs. *SPE* 3 (1), 60–67.
- van Dijke, M. I. J., Sorbie, K. S., 2002. The relation between interfacial tensions and wettability in three-phase systems: Consequences for pore occupancy and relative permeability. *J. Pet. Sci. Eng.* 33 (1–3), 39–48.
- van Dijke, M. I. J., Sorbie, K. S., 2003. Three-phase capillary entry conditions in pores of noncircular cross-section. *J. Coll. Int. Sci.* 260, 385–397.
- Virnovsky, G. A., 2004. Private communication.
- Virnovsky, G. A., Iversen, J. E., 1999. Measurement and interpretation of three-phase capillary pressure by centrifuge. Paper presented at the 10th European Symposium on Improved Oil Recovery, Brighton, UK, Aug. 18–20 .
- Whitson, C. H., Brulè, M. R., 2000. Phase Behavior. Vol. 20 of Henry L. Doherty series Monograph / SPE. Society of Petroleum Engineers, Richardson, TX.
- Yang, S.-Y., Hirasaki, G., Basu, S., Vaidya, R., 1999. Mechanisms for contact angle hysteresis and advancing contact angles. *J. Pet. Sci. Eng.* 24, 63–73.
- Zhou, D., Blunt, M., 1998. Wettability effects in three-phase gravity drainage. *J. Pet. Sci. Eng.* 20, 203–211.